

Monte Carlo simulation of free radical production under keV photon irradiation of gold nanoparticle aqueous solution. Part I: Global primary chemical boost

Floriane Poignant, Hela Charfi, Chen-Hui Chan, Elise Dumont, David Loffreda, Etienne Testa, Benoît Gervais, Michael Beuve

► To cite this version:

Floriane Poignant, Hela Charfi, Chen-Hui Chan, Elise Dumont, David Loffreda, et al.. Monte Carlo simulation of free radical production under keV photon irradiation of gold nanoparticle aqueous solution. Part I: Global primary chemical boost. Radiation Physics and Chemistry, Elsevier, 2020, 172, pp.108790. 10.1016/j.radphyschem.2020.108790 . hal-02498384

HAL Id: hal-02498384

<https://hal.archives-ouvertes.fr/hal-02498384>

Submitted on 30 Nov 2020

HAL is a multi-disciplinary open access archive for the deposit and dissemination of scientific research documents, whether they are published or not. The documents may come from teaching and research institutions in France or abroad, or from public or private research centers.

L'archive ouverte pluridisciplinaire **HAL**, est destinée au dépôt et à la diffusion de documents scientifiques de niveau recherche, publiés ou non, émanant des établissements d'enseignement et de recherche français ou étrangers, des laboratoires publics ou privés.

Journal Pre-proof

Monte Carlo simulation of free radical production under keV photon irradiation of gold nanoparticle aqueous solution. Part I: Global primary chemical boost

Floriane Poignant, Hela Charfi, Chen-Hui Chan, Elise Dumont, David Loffreda, Étienne Testa, Benoit Gervais, Michaël Beuve

PII: S0969-806X(19)31604-4

DOI: <https://doi.org/10.1016/j.radphyschem.2020.108790>

Reference: RPC 108790

To appear in: *Radiation Physics and Chemistry*

Received Date: 18 December 2019

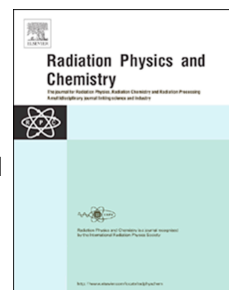
Revised Date: 15 February 2020

Accepted Date: 18 February 2020

Please cite this article as: Poignant, F., Charfi, H., Chan, C.-H., Dumont, E., Loffreda, D., Testa, É., Gervais, B., Beuve, Michaël., Monte Carlo simulation of free radical production under keV photon irradiation of gold nanoparticle aqueous solution. Part I: Global primary chemical boost, *Radiation Physics and Chemistry* (2020), doi: <https://doi.org/10.1016/j.radphyschem.2020.108790>.

This is a PDF file of an article that has undergone enhancements after acceptance, such as the addition of a cover page and metadata, and formatting for readability, but it is not yet the definitive version of record. This version will undergo additional copyediting, typesetting and review before it is published in its final form, but we are providing this version to give early visibility of the article. Please note that, during the production process, errors may be discovered which could affect the content, and all legal disclaimers that apply to the journal pertain.

© 2020 Published by Elsevier Ltd.



Floriane Poignant, Methodology, Software, Validation, Investigation, Writing – Original – draft, Writing – Review and editing

Hela Charfi, Software, Validation, Investigation, Writing – Review and editing

Chen-Hui Chan, Writing – Review and editing

Elise Dumont, Writing – Review and editing

David Loffreda, Writing – Review and editing

Etienne Testa, Conceptualization, Writing – Review and editing, Supervision, Funding acquisition

Benoit Gervais, Conceptualization, Software, Writing – Original, Writing – Review and editing

Michaël Beuve, Conceptualization, Methodology, Software, Writing - Original, Writing – Review and editing, Supervision, Funding acquisition

Monte Carlo simulation of free radical production under keV photon irradiation of gold nanoparticle aqueous solution. Part I: global primary chemical boost.

Floriane Poignant^a, Hela Charfi^a, Chen-Hui Chan^b, Elise Dumont^{b,d}, David Loffreda^b, Étienne Testa^a, Benoit Gervais^c, Michaël Beuve^a

^aUniv. Lyon, Univ. Claude Bernard Lyon 1, CNRS/IN2P3, IP2I Lyon, F-69622, Villeurbanne, France.

^bUniv. Lyon, Ens de Lyon, CNRS UMR 5182, Université Claude Bernard Lyon 1, Laboratoire de Chimie, F-69342 Lyon, France

^cCIMAP, unité mixte CEA-CNRS-ENSICAEN-UCBN 6252 BP 5133, F-14070 Caen, Cedex 05, France

^dInstitut Universitaire de France, 5 rue Descartes, 75005 Paris

Abstract

The use of gold nanoparticles to enhance radiation therapy efficiency has been thoroughly investigated over the past two decades. While theoretical studies have mostly focused on physical mechanisms and dose enhancement, studies of free radical production are scarce. In this work, we investigated the primary yield of free radicals ($\bullet\text{OH}$ and H_2O_2) induced by 20-90 keV monoenergetic photons, for small GNPs concentrations. Our study is based on a Monte Carlo approach which enables electron transport down to low energy, both in water and in gold. We obtained, for a gold concentration of $1 \text{ mg} \cdot \text{mL}^{-1}$, an average chemical enhancement varying from 6 to 14 %, depending mostly on the photon energy and, to a lesser extent, on the chemical species and size of the GNP. This enhancement is strongly correlated to the dose deposition enhancement, although not strictly proportional. While supporting the hypothesis that therapeutic efficiency of GNPs may not simply be explained by an overproduc-

Email address: m.beuve@univ-lyon1.fr (Michaël Beuve)

tion of free radicals in the early stage, our simulation provides inputs for further macroscopic simulations, including cumulative track effects and potentially GNP chemical reactivity.

Keywords: gold nanoparticles, photon irradiation, water radiolysis, radiation-chemical yields, Monte Carlo simulation

1. Introduction

The use of nanoparticles in cancer therapy has been of high interest since the pioneering work of Hainfeld *et al.* [1], demonstrating the efficacy of the combination of injected gold nanoparticles (GNPs) with X-ray irradiation for mice with EMT-6 carcinoma tumors. The mechanisms of nanoparticle enhanced radiotherapy may originate from complex physico-chemical and biological steps which depend on many parameters, such as the composition of the NP, the energy of the irradiation beam, and the biological system [2]. The relative contribution of these different steps, and the connection between them, still needs to be clarified [3]. As the time and spatial scales involved in the early mechanisms are very short, a clear experimental identification of the origin of the effect is not straightforward and remains under investigation. In this context, theoretical approaches, such as Monte Carlo (MC) simulations, may help to better understand how early physical and chemical stages could impact a biological system and lead to cell death enhancement.

Many MC studies have focused on the physical stage, to study the dose deposition distribution at tumor scale [4, 5, 6, 7, 8, 9, 10, 11, 12, 13], and at both cellular and sub-cellular scale [14, 15, 16, 17, 18]. Both keV and MeV photon energies were investigated [19, 20], and hadrontherapy combined with GNPs was also studied [21]. Nanoparticles made of heavy atoms with high atomic number (Z) such as metals are more efficient than water at absorbing low energy (keV) X-rays. For energies up to ~ 500 keV, the photo-electric effect dominates in metals, resulting in a particularly high probability of photon-metal inter-

action compared to photon-water interaction, and consequently an increase in
 25 the macroscopic (tumor) dose deposition [4, 5, 6, 7, 8, 9, 10, 11, 12, 13]. In
 particular, studies showed that a significant dose enhancement may occur when
 the concentration of GNP inside the tumor is high enough. For example, 7
 mg gold/g tumor could result in a dose enhancement as high as 110 % for 140
 kVp and 70 % for I-125 gamma rays [22]. Strategies were discussed to use
 30 GNPs as contrast agents for human eye choroidal melanoma [23], prostate can-
 cer brachytherapy [24], ARC therapy applied to brain tumors [12] or as a tumor
 vascular disrupting agents (VDAs) [25, 26, 27, 28, 21]. Another study suggested
 the use of radioactive low-dose rate GNPs, to improve the current low-dose rate
 brachytherapy strategies [29].

35 *In solution* irradiation experiments with colloidal GNPs [30, 31, 32, 33, 34, 35,
 36] or in presence of bio-molecules [37, 38, 39, 40, 41, 42] put in light the impor-
 tance of the chemical stage. In particular, the use of plasmid DNA evidenced
 that the enhancement of DNA single strand breaks was dependent on the en-
 ergy of the incident photon in the keV range[40, 42], the concentration of GNPs
 40 [40], the chemical environment of the solution and in particular its scavenging
 ability [38, 39, 42], and the proximity between the GNPs and the biomolecules
 [38, 41]. Large increase of reactive oxygen species (ROS) production was also
 measured with *in vitro* probes for cells irradiated in presence of GNPs, com-
 pared to cells irradiated without GNPs [43, 44], although it is unclear whether
 45 it is directly produced by the interaction of radiations with GNPs, or indirectly
 by the interaction of the GNPs with cellular components. Overproduction of
 free radicals during water radiolysis induce an oxidative stress which may result
 in cells failing to maintain normal physiological redox-regulated functions [45].
 Dramatic effects, such as oxidative modification of proteins, lipid peroxidation,
 50 DNA-strand break, etc. [45], result in cell death.

As pointed by Her *et al.* [2] in a recent review, the chemical stage has yet
 not been fully investigated. While there have been many MC studies on the
 physical step, to our knowledge only a few MC studies have been conducted

on the ROS enhancement for GNP-enhanced radiation therapy [46, 47, 48],
 55 although it was suggested to be a crucial step that may connect the physical
 effect to the biological consequences [3, 29]. In particular, no systematic study
 of free radical production has been performed for GNP-enhanced radiotherapy
 in the range of keV photon energies.

The goal of this work is thus to investigate the impact of GNPs on the pro-
 60 duction of free radicals for keV photon irradiation in water by means of MC
 simulations. We shall compute the yield Y_X of chemical species X , for a given
 concentration C_{NP} of GNPs homogeneously distributed in a volume of water,
 irradiated by a beam of monoenergetic photons in the range 20-90 keV. As most
 of the probes of the aforementioned studies measured either hydroxyl radicals
 65 ($\bullet\text{OH}$) and hydrogen peroxide (H_2O_2), this study focused on these two species.
 In particular, we aim to estimate how the increase of dose deposition during
 the physical stage, including the Auger cascade, affects the chemical radiolytic
 yield, for an average photon impact. Our results provide values of the boost of
 chemical species delivered by primary photon impacts at short time following
 70 the impact, which we shall refer to as the primary boost. It may be used as
 a inputs for further macroscopic simulations, including cumulative track effects
 and potentially GNP chemical reactivity.

This paper is organized as follows. In section 2, the MC tool and system con-
 sidered are presented. The average dose deposition and the radical species pro-
 75 duction are studied in section 3 as a function of photon energy, size of the GNP
 and type of chemical species. Section 4 discusses and concludes on the results,
 with regard to theoretical and experimental results available in the literature.

2. Material and methods

2.1. General considerations

80 *A. Simulation strategy.* Our solution sample represents a volume of liquid water
 containing a homogeneous concentration C_{NP} of GNPs. In such a sample, we

consider a cubic sub-volume of interest V placed at a depth from the beam entrance so that the flux of charged particles (e.g. electrons) entering the volume is equal to the flux of charged particles leaving the volume. Such a condition is often referred to as the equilibrium of charged-particles. Under this constraint, the length of V is assumed sufficiently small with respect to the photon mean free path, and sufficiently close to the beam entrance to ensure that the photon beam remains monoenergetic. In such conditions, it is possible to neglect the photon beam transport and attenuation. Therefore, in our simulation, V is irradiated by a beam of monoenergetic photons, for which a prescribed reference dose D in water (i.e., without GNPs) can be defined. For such a volume, the mean number of interactions can directly be calculated both in water and in the GNPs, based on D . Photon impacts can be considered homogeneously distributed in each material, according to their total photon absorption cross section [49]. Such a volume is typically of what has been used for radiation chemistry [30].

While desirable, a direct simulation of irradiation of a large volume containing a large number of GNPs is unfortunately not possible, because the computational cost of chemical simulations scales as the square of the number of chemical species.

We thus added the following approximations and considerations. First, we simulated the physical and chemical processes in V , applying periodic boundary conditions (see Fig. 1) to achieve charged-particle equilibrium, as defined above [49]. The dimensions of V were larger than a single-track extension, and we thus avoided the spurious interaction of a track with its periodic image.

Secondly, we calculated radical production track-by-track, ignoring the interaction between the radicals generated in two different tracks. This consideration is consistent with the results obtained with most standard experimental methods used to measure radiation-chemical yields. Such experiments consist in using scavengers to reduce inter-track effects, or in applying medium renewal at a rate that is fast enough compared to the dose rate. In such conditions, the concentration of radicals is proportional to the number of absorbed photons, and

thus to the prescribed dose D . We thus defined the average yield of radicals as the yield obtained for 1 μ s time t evolution in a single-photon track, and then averaged over a large number of tracks. We expect our approach to be valid
 115 under relatively low flux conditions. In this case the relative effect of GNP with respect to pure water is definitely well estimated. For more accuracy under high flux conditions, the track overlap should be taken into account.

Finally, we limited our study to a concentration C_{NP} of GNPs sufficiently low to neglect the probability that a single track overlap simultaneously two GNPs.
 120 For a GNP concentration of $1 \text{ mg} \cdot \text{mL}^{-1}$, we typically find that the probability for a track created in water to hit a GNP is of a few percents. Another working hypothesis is that the GNP does not participate to the chemical stage. We assume that they are chemically inert. Moreover, up to 1 μ s, the probability that chemical species react with a GNP is rather small, due to limited diffusion
 125 and to the fact that most of the particles are created in water far from any GNP for the considered concentration of $1 \text{ mg} \cdot \text{mL}^{-1}$. It was therefore possible to consider only three kinds of single-track event following a photo-ionization: the case (W) where a photon interacted with water and did not lead to secondary particles interacting with the GNP, the case (W+NP) where a photon interacted
 130 with water and led to at least one secondary particle interaction with the GNP and the case (NP) where the photon directly interacted with the GNP. They are referred to as (1,2,3), corresponding respectively to (W,W+NP,NP), and illustrated in Fig. 1. As detailed in the Appendix A, the probability that a track hits two or more GNP is negligible. The final yield was obtained as a sum
 135 of these 3 contributions, weighted by their respective probability.

B. Investigated parameters. Four GNP radii (5 nm, 12.5 nm, 25 nm and 50 nm) and energies from 20 to 90 keV were chosen to study the impact of the GNP size and photon energy on chemical species yields. The half length of V was therefore comprised between 15 μ m at 20 keV to 160 μ m at 90 keV. This ensures that the
 140 dimensions of V are lower than the photon mean free path, which is typically

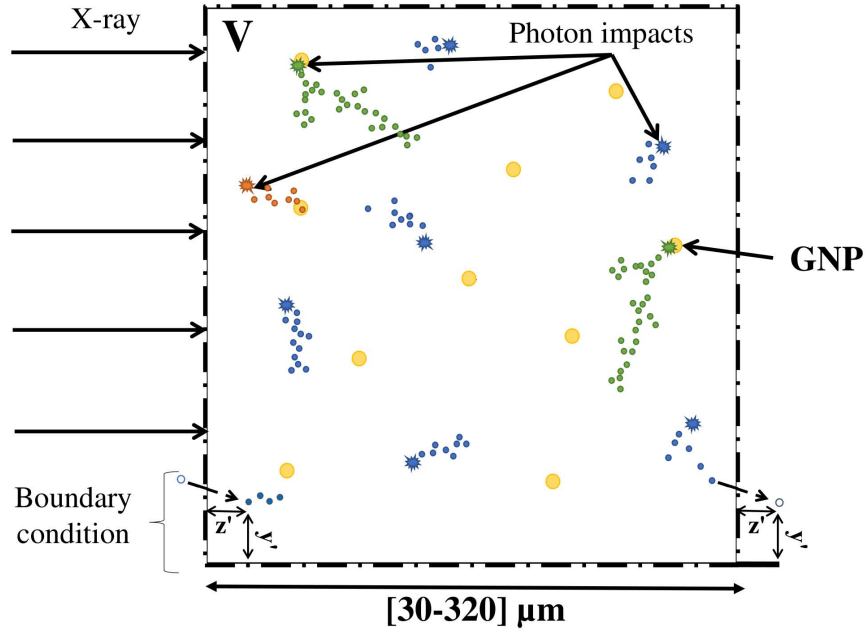


Figure 1: Schematic view of the cubic volume of interest V considered for radical species simulation. The number of photon impacts are computed in each medium (water and GNPs) and randomly distributed in each corresponding volume. Sub-contributions are represented in blue (W), orange (W+NP) and green (NP).

of the order of 1 cm at 20 keV. The different calculations were all performed for a GNP concentration of $1 \text{ mg} \cdot \text{mL}^{-1}$. This concentration is in the range of reported *in solution* [30, 31, 32, 33, 34] and *in vitro* [50, 51, 52] experimental concentrations. For comparison with the results from the literature, we reported

145 different quantities in Tab. 1. We define $n(E)$ (respectively $f(E)$) the number (respectively proportion) of ionized GNPs in a cubic volume of length equal to $10 \text{ } \mu\text{m}$ (of the order of the size of a cell), for photon energy E , 1 Gy irradiation and GNP concentration of $1 \text{ mg} \cdot \text{mL}^{-1}$. We found that $n(E)$ was equal to 6 and 45 for E equal to 80 and 20 keV respectively. $f(E)$ is extremely small for

150 5 nm GNPs regardless of the photon energy, while it is close to 50 % for 50 nm GNPs and E equal to 20 keV.

R_{NP}	5 nm	12.5 nm	25 nm	50 nm
GNP concentration in $\text{mg} \cdot \text{mL}^{-1}$	1			
GNP concentration in nM	164	10	1.3	0.16
GNP concentration in $\text{NP} \cdot \text{cm}^{-3}$	9.9×10^{13}	6.3×10^{12}	7.9×10^{11}	9.9×10^{10}
Average distance between 2 GNPs (nm)	216	541	1080	2160
	Cellular volume : cube of $10 \times 10 \times 10 \mu\text{m}^3$			
Number of GNPs	$\sim 100\ 000$	$\sim 6\ 000$	~ 800	~ 100
$f(E)$ (%) for $E = 80$ keV	0.01	0.1	0.77	6.15
$f(E)$ (%) for $E = 20$ keV	0.05	0.71	5.66	45.28
$n(E)$ for $E = 80$ keV	6			
$n(E)$ for $E = 20$ keV	45			
Ratio volume GNP over volume water	$\sim 5 \times 10^{-5}$			

Table 1: Concentration of GNP for various metrics and various GNP sizes. The average distance between two GNPs was calculated assuming that GNPs are homogeneously distributed in a cubic network.

2.2. Monte Carlo simulation for dosimetry and water radiolysis

The irradiation of the volume V was modeled by 3 distinctive stages. During the physical stage, particles traveling through the media deposit energy, which provided us dosimetric quantities. This physical stage is followed by a physico-chemical and a chemical stage leading to the creation of many highly reactive chemical species. Up to the beginning of the chemical stage, the track structure is highly heterogeneous. Hence the chemical reactions cannot be described by simple first or second order kinetic equations [53]. Thus, at short time, Monte Carlo (MC) techniques are required to calculate radiation-chemical yields as a

function of time. We used the MC code MDM [54, 55, 56, 57], which performs an event-by-event tracking of electrons and ions. Formerly known as the LQD code [54], it was originally developed to track ions and low energy electrons and products of chemical reactions down to very low energies (thermalization) in pure liquid water. It was later modified to consider various heterogeneous domains such as metallic media, which has led to emergence of the new branch MDM, i.e. for MeDiuM [56, 55]. A full description of the MC models and constant of chemical reactions used in the present work are available elsewhere [54, 55, 58], and are briefly presented in this section.

2.2.1. Physical stage

The physical stage occurs in the first few fs after each photon absorption. At the end of this stage, the water molecules may be either excited (H_2O^*) or ionized (H_2O^+ , H_2O^{2+} and H_2O^-), and the medium contains thermalized electrons (e_{th}). Our model [54] consisted in an event-by-event tracking of particles in the different media (water or gold). The energy deposited inside GNPs was considered as lost energy, and vacancies or electrons that were contained within GNPs were no longer tracked at the end of this stage. The next paragraphs give a brief overview of the interactions considered for photons and electrons with the media of interest (water and gold).

A. Photons. Only the photoelectric effect and the Compton effect were taken into account as they are predominant at these energies. The photoelectric cross sections were taken from the XCOM database [59]. In our simulation, the angular distribution of the ejected photoelectron was assumed to be isotropic. For the Compton effect, the cross section was calculated using the differential cross section based on the Klein-Nishina formula [60], given by,

$$\frac{d\sigma}{dE_{\text{kin}}} = \frac{\pi r_e^2}{m_e c^2 \gamma^2} \left(2 + \frac{s^2}{\gamma^2 (1-s)^2} + \frac{s}{1-s} \left(s - \frac{2}{\gamma} \right) \right), \quad s = \frac{E_{\text{kin}}}{h\nu} \quad (1)$$

with E_{kin} the energy of the recoil electron, $\gamma = \frac{h\nu}{m_e c^2}$, $r_e = 2.818 \times 10^{-15}$ m is the classical radius of the electron, $h\nu$ is the energy of the incoming photon and $m_e c^2 = 511$ keV is the electron mass energy. The total cross section was then obtained by integrating Eq. 1 from 0 to the maximum energy transfer $E_{\text{kin,max}}$,
 190 given by

$$E_{\text{kin,max}} = h\nu \left(\frac{2\gamma}{1 + 2\gamma} \right). \quad (2)$$

B. Electrons. A full description of the model for gold-electron interactions is given in the study by Poignant *et al.* [55], and for water-electron interactions in the study by Gervais *et al.* [54]. Briefly, we modeled the full electronic cascade following the primary photon interaction down to thermalization, accounting
 195 for inelastic (ionizations, electron and vibrational excitations, electronic attachment) and elastic interactions in both gold and water. Regarding ionization, a solid state formalism was applied for outer-shell electrons of gold, while an atomic model was applied for both water and inner-shell electrons of gold. We emphasize that in this study, the cross sections do not depend on the size and
 200 shape of the nanoparticles. In particular, plasmons resonances correspond to the ones of bulk gold. The possible effects of surface plasmon resonance modification due to the GNP shape and size or due to GNP coupling with the surrounding medium are not taken into account. In particular, plasmons resonances correspond to the ones of bulk gold. For an accurate evaluation of radiation-
 205 chemical yields, it is mandatory to account for de-excitation and recombination processes. We considered Auger de-excitation both in water and in gold. For gold [55], data were taken from the EADL library. Emitted fluorescence photons were not tracked and therefore did not lead to additional energy deposition in the volume. Although these photons might carry a large amount of the initial
 210 photon energy after a GNP ionization, most of them had an energy larger than 10 keV. Hence, their mean free path in water was larger than the dimensions of the volume of interest, meaning their contribution to the radiation-chemical

yield was negligible. The small probability of thermalized electron recombination with a water vacancy was taken into account, resulting in an excited water molecule [61]. To ensure a consistent tracking of electron kinetic energy when
 215 changing medium, both materials were described by a mesoscopic potential of values equal to -1.30 eV for water and -10.04 eV for gold. The kinetic energy of the electron was modified when crossing the water-GNP interface, on the basis of the mesoscopic potential difference between the two media.

220 2.2.2. Physico-chemical stage in water

This stage models the relaxation of water molecules leading to the production of primary chemical species, occurring from 10^{-15} to 10^{-12} s after the interaction of a photon with the media. The molecules may dissociate, in which case the two products were generated at a given distance from one to another to account
 225 for their kinetic energy. The different branching ratios of each molecular rearrangement are provided in another work [54]. They were not influenced by the presence of the GNP. At the end of this stage, several chemical species were produced, with a majority of e_{aq}^- , H_3O^+ and $\bullet OH$. Note that chemical species did not diffuse during this stage.

230 2.2.3. Chemical stage in water

At 10^{-12} s, the primary chemical species start to diffuse and may react with each other. Our simulation tracked all chemical species up to 10^{-6} s. At the end of the chemical stage, the so-called steady state is reached and the radiolytic yields reach asymptotic values [54, 53]. Our method used to calculate the yields
 235 is described elsewhere [54, 62, 58]. The simulation parameters were taken from the work by Frongillo *et al.* [53]. More than fifty reactions were possible, and are listed in the work by Coliaux *et al.* [58]. During this stage, interaction of chemical species with the GNP were not considered.

2.3. Calculated quantities

240 2.3.1. Radiation-chemical yield in water

Defining $R_X(D)$ the mean number of species X produced in a volume V for a dose of irradiation D , we decomposed $R_X(D)$ as the sum of the 3 contributions as illustrated in Fig. 1,

$$R_X(D) = R_{X,1}(D) + R_{X,2}(D) + R_{X,3}(D) \quad (3)$$

Given our hypotheses introduced in section 2.1, each contribution $R_X(D)$ is the
 245 dose weighted average over a large number of single-tracks, associated to the selected event i ,

$$R_{X,i}(D) = n_i(D)\bar{R}_{X,i}^1, \quad \text{with } i \in [1, 2, 3]. \quad (4)$$

$\bar{R}_{X,i}^1$ is the average number of chemical species X obtained for a single-track event i . $n_i(D)$ is the mean number of absorbed photon leading to event i for the given dose D . Note that $n_1(D) = n_2(D)$, as both represent the mean number
 250 of photon interactions in water. They are expressed as follows,

$$\begin{cases} n_1(D) = n_2(D) = F(D)\sigma_W\rho_W V(1 - C_{NP}V_{NP}) \\ n_3(D) = F(D)\sigma_{NP}\rho_{NP} V C_{NP}V_{NP}, \end{cases} \quad (5)$$

with $F(D)$ the fluence of the beam which is linear with the dose D , V the total volume, V_{NP} the volume of one nanoparticle, C_{NP} the GNP concentration, σ_x the total cross section for photon-interaction in the medium x , ρ_x the density of the medium x .

255 Each number of chemical species $\bar{R}_{X,i}^1$ does not depend on the dose but depends on the chosen event i , and as such depends on the GNP concentration, as detailed in Appendix A. It is obtained by averaging the number of chemical species obtained per single-track event i over a large number of single-track

events. The most straightforward strategy to obtain such events is to generate
 260 a photon impact in a sample consisting of a random array of GNPs distributed
 in water.

The yield Y_X in $\text{nmol} \cdot \text{J}^{-1}$ is deduced from $R_X(D)$ as follows,

$$Y_X = \frac{10^{12}}{DV \times \rho_W \times N_a} R_X(D) \quad (6)$$

with Y_X expressed in $\text{nmol} \cdot \text{J}^{-1}$, D the dose ($\text{J} \cdot \text{kg}^{-1}$), V the total volume
 (cm^3), ρ_W the water density ($\text{g} \cdot \text{cm}^{-3}$), N_a the Avogadro number. Note that,
 265 as the chemical species number was proportional to D , the resulting yields
 are independent of the dose D . Moreover, since the concentration of GNPs
 is sufficiently low, the contributions $R_{X,2}(D)$ and $R_{X,3}(D)$ are proportional to
 C_{NP} , as shown in Appendix A. This would be different if the concentration was
 larger. Alternatively, as events of type 2 (W+NP) are rare events, it is possible
 270 to fasten the simulation by using a biasing method. Our strategy consisted
 in first generating a track in pure water. We then calculated a position for
 which the track interacted with the GNP, along with the probability for this
 track to interact with the GNP. The track was re-generated, using the same
 seed, but translating it to force the interaction of secondary particles to occur.
 275 The probability for the track to interact with the GNP was then used as a
 weight coefficient, as detailed in Appendix A. Note that replacing the GNPs by
 nanoparticles made of water led to the same yield as for pure water.

2.3.2. Energy deposition in water

After irradiating a volume of water containing C_{NP} GNPs, dosimetric outputs
 280 consisted in the spatial distribution of all low-energy electrons and ionized or
 excited water molecules. The track-by-track method, previously introduced for
 the calculation of the average yield of chemical species, was also applied for the
 calculation of the dose deposition. For a concentration C_{NP} of GNPs and a

prescribed dose D , we find a dose deposition D' ,

$$D' = \sum_i n_i(D) \overline{D}_i^1 \quad \text{with } i \in [1, 2, 3] \quad (7)$$

285 with \overline{D}_i^1 the average dose for the track type i . As for the calculation of chemical-radiation yields, the volume of interest V used to obtain the average dose varied from 30^3 to $320^3 \mu\text{m}^3$, according to the photon energy.

2.3.3. Statistical uncertainty

For the contribution i and the chemical species X , associated with N_i the number of tracks of type i simulated, the standard deviation $\sigma_{R_X(D)}$ of the number of chemical species $R_X(D)$ is,

$$\sigma_{R_X,i(D)} = \sqrt{\frac{1}{N_i} \sum_{t=1}^{N_i} \left(n_i(D) R_{X,i}^t - R_{X,i}(D) \right)^2} \quad (8)$$

with $R_{X,i}^t$, the number of chemical species X obtained for the track t . The final statistical uncertainty, for the number of chemical species, reads,

$$\sigma_{R_X(D)} = \sqrt{\left(\frac{\sigma_{R_{X,1}}}{\sqrt{N_1}} \right)^2 + \left(\frac{\sigma_{R_{X,2}}}{\sqrt{N_2}} \right)^2 + \left(\frac{\sigma_{R_{X,3}}}{\sqrt{N_3}} \right)^2} \quad (9)$$

Similar uncertainties were obtained for the energy deposition, the yields and radial quantities. Each results were displayed with error bars that were set to $\pm \sigma_{R_X}$.

3. Results

3.1. Energy deposition

Fig. 2 represents dosimetric quantities for $1 \text{ mg} \cdot \text{mL}^{-1}$ of GNPs and for a prescribed dose $D = 1 \text{ Gy}$. The variation of the dose for pure water is a purely

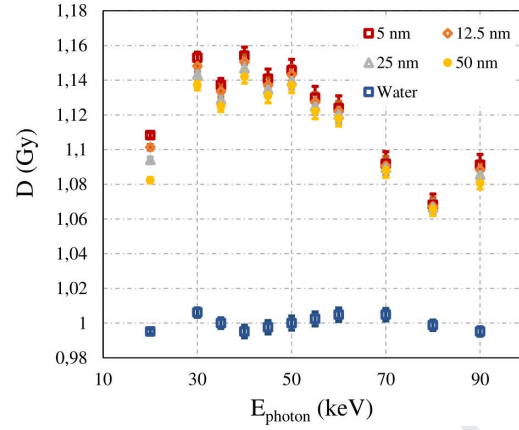


Figure 2: Dose D' as a function of the photon energy E_{photon} , for $C_{\text{NP}} = 1 \text{ mg} \cdot \text{mL}^{-1}$, various GNP radii, a prescribed dose to water $D = 1 \text{ Gy}$.

statistical effect. The increase of the dose due to GNPs is comprised between $\sim 6 \%$ and $\sim 16 \%$ depending on the photon primary energy. For energy larger than 20 keV, there is an increase of the dose deposition with increasing photon energy, as the photo-electron energy is higher and lose therefore less energy within the GNP. Then, the relative increase goes down to 6 % at 80 keV as the ratio between gold and water photon absorption cross section decreases. The maximum is reached around 40-50 keV. At 90 keV, there is small increase of the dose due to the increase of the photo-electric cross section of gold by K-shell ionization. It can be noted that the increase is relatively independent of the GNP radius, except for low energy photons, in which case the energy deposited in the GNP is significantly more important for large GNPs. At 20 keV, GNP with a 50 nm (respectively 5 nm) radius absorbs $\sim 25 \%$ (respectively 5 %) of the total photon energy following a photo-ionization. It is equal to less than 10 % for all radii beyond 40 keV. Moreover, the events W+NP do not induce much energy loss by energy absorption in the GNPs, because the track initiated in water leads mostly to dose deposition in water even though a GNP has been hit. Thus, on average, at these photon energies, the contribution coming from photon interaction with water ($t_{\text{W+NP}} + t_{\text{W}}$) can be replaced by a contribution of pure

water. Finally, we noticed that Auger electrons emitted from a GNP contribute
 320 to less than 4 % of the total dose deposition at $1 \text{ mg} \cdot \text{mL}^{-1}$. As detailed in
 Appendix A, the relative increase of the dose may be linearly extrapolated at
 larger GNP concentrations, up to few tens of $\text{mg} \cdot \text{mL}^{-1}$.

3.2. Radiation-chemical yields in water

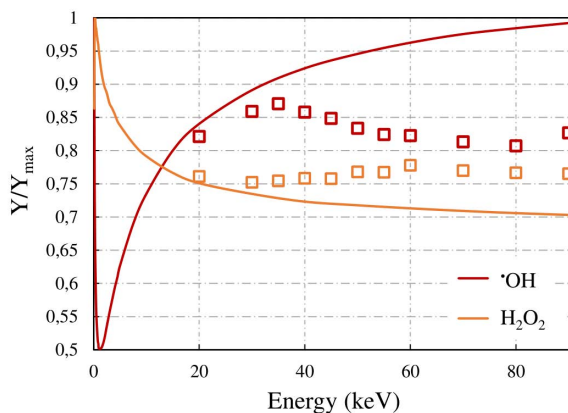


Figure 3: Radiation-chemical yields of H_2O_2 and $\bullet\text{OH}$ as a function of the primary electron (solid line) or photon (squaredots) energy in pure water, at $1 \mu\text{s}$, normalized to the respective maximal values.

Fig. 3 represents the normalized radiation-chemical yields of H_2O_2 and $\bullet\text{OH}$
 325 obtained for electron and photon irradiation without GNPs, as a function of the
 incident particle energy at $1 \mu\text{s}$ following the primary interaction. Both yields
 are correlated as the production of H_2O_2 is mainly due to the recombination of
 two $\bullet\text{OH}$. The yields are normalized to the maximal values: $109 \text{ nmol} \cdot \text{J}^{-1}$ for
 H_2O_2 and $246 \text{ nmol} \cdot \text{J}^{-1}$ for $\bullet\text{OH}$. The electron and photon results would be
 330 nearly identical if only the photoelectric effect took place.

For electron irradiation, there is first a sharp increase of H_2O_2 production at
 very low primary electron energies ($< 300 \text{ eV}$). Then, H_2O_2 yield decreases for
 primary electron energies increasing up to $\sim 20 \text{ keV}$, due a lower recombination
 probability with increasing energy. Finally, it reaches a plateau, whose value

335 at 90 keV is ~ 70 % of the maximum value. On the contrary, $\bullet\text{OH}$ yield first strongly decreases down to 50 % of its maximal value, before increasing again and reaching a plateau that is nearly equal to the maximal value at 90 keV. This variation for electron impact reflects the change of the track structure as the projectile energy changes.

340 For photon irradiation without GNP, there is a small fluctuation of the radiation-chemical yields depending on the photon energy. From 20 to 35 keV, $\bullet\text{OH}$ yield increases from $203.0 \pm 0.4 \text{ nmol} \cdot \text{J}^{-1}$ up to $215.2 \pm 0.8 \text{ nmol} \cdot \text{J}^{-1}$. At these energies, the photo-electric effect remains non negligible. Consequently, the primary electron generated following a photon interaction in water has an energy
 345 that is nearly equal to the photon energy. We therefore obtain yields that are very close to those obtained for electron irradiation. As the photon energy increases, the Compton effect starts dominating [59]. Following a Compton event in water at such energies, the primary electron energy distribution is rather flat up to a maximum value significantly smaller than the incoming photon energy
 350 (typically ~ 20 keV for a 90 keV photon). Consequently, many primary electrons are emitted in the 0-20 keV range, for which $\bullet\text{OH}$ production is reduced. We therefore observe a decrease of $\bullet\text{OH}$ yield down to $199.5 \pm 0.9 \text{ nmol} \cdot \text{J}^{-1}$ and an increase of H_2O_2 production. Then, for a photon energy of 90 keV, the primary electron energy tends to be higher on average, and the proportion of
 355 primary electrons emitted at very low energies is reduced in proportion, thus favoring back $\bullet\text{OH}$ production. This result for pure water is consistent with a previous study reported in the literature [63]

Fig. 4 displays the absolute ((a) and (b)) and relative to pure water ((c) and (d)) yields of H_2O_2 and $\bullet\text{OH}$ at 10^{-6} s, as a function of the primary photon
 360 energy (in keV), for a GNP concentration of $1 \text{ mg} \cdot \text{mL}^{-1}$, for different R_{NP} .

Regarding the yields in the presence of GNPs, both H_2O_2 and $\bullet\text{OH}$ yields follow similar trends with regard to the photon primary energy variation and behave alike the dose. There is first an increase of the yield enhancement from ~ 11 to ~ 14 % for H_2O_2 and ~ 8 to ~ 14 % for $\bullet\text{OH}$, when the photon energy increases

365 from 20 to 40-50 keV. Then, the enhancement decreases down to $\sim 6\%$ for H_2O_2
 and $\sim 7.5\%$ for $\bullet\text{OH}$, when the photon energy increases to 80 keV. At 90 keV,
 both enhancements increase back to $\sim 8-9\%$. Interestingly, the enhancements
 are slightly different depending on the chemical species. In particular, H_2O_2 is
 370 favored at lower photon energies while $\bullet\text{OH}$ is favored at higher energies. This
 is explained by the photo-electron energy dependency of the radiation-chemical
 yields as displayed in Fig. 3. When the primary photon energy and thus photo-
 electron energy is low (from 20 to 35 keV), ionizations in tracks are denser and
 thus recombination becomes more important, leading to a higher H_2O_2 yield.

It may also be noted that, just as for the dose enhancement, the radius of the
 375 GNP does not impact much the radiolytic enhancement. Although, at 20 keV,
 the enhancement significantly varies from $\sim 9\%$ to $\sim 12\%$ with radius from 50 to
 5 nm, this difference becomes negligible at higher energies. This is simply due
 to energy absorption within the GNP, which decreases with increasing photon
 energy.

380 4. Discussion and conclusion

Over the past two decades, experimental and theoretical studies have shown
 the ability of gold nanoparticles (GNPs) to increase the efficiency of radiation
 therapy. For low-energy (keV) photons, this enhancement partially results from
 an increase of the dose deposition, due to a higher cross section for gold-photon
 385 interaction compared to water-photon interaction. While Monte Carlo (MC)
 simulations have widely been used to quantify this dose boost [4, 5, 6, 7, 8, 9,
 10, 11, 12, 13, 14, 15, 16, 17, 18, 19, 20, 21], the impact of GNPs on radical
 species production has yet hardly been investigated. In the present study, we
 investigated the average primary boost of chemical species yields (H_2O_2 and
 390 $\bullet\text{OH}$) under keV photon irradiation of water containing a concentration C_{NP} of
 GNPs by mean of MC simulation. The variation of radiation-chemical yields
 was studied with regard to photon energy (20 to 90 keV) and GNP radius (5 to

50 nm), at 1 μ s following the primary photon interaction.

For 1 $\text{mg} \cdot \text{mL}^{-1}$ of gold, we obtained a relative dose increase which varied
 395 from ~ 6 to ~ 16 %, depending mostly on the photon energy but also, to a
 lesser extent, on the GNP radius for the lowest photon energies. Most of the
 energy was deposited by the photo-electron, while the contribution of Auger
 electrons overall remained below 4 %. For sufficiently low GNP concentration,
 this increase was linear with the GNP concentration up to a few tens of $\text{mg} \cdot$
 400 mL^{-1} . Values obtained for 1 $\text{mg} \cdot \text{mL}^{-1}$ may therefore be linearly extrapolated at
 other GNP concentrations. The obtained dosimetric results are consistent with
 those reported in the literature. For instance, Lechtman *et al.* [64] reported that,
 for 5-100 nm diameter GNPs and a monoenergetic source of Pd-103 (20.48 keV),
 ~ 6 -8 $\text{mg} \cdot \text{mL}^{-1}$ of GNPs would be required to double the dose. In comparison,
 405 at 20 keV and assuming a linear extrapolation of our results with regard to GNP
 concentration, we find that 8.8-11 $\text{mg} \cdot \text{mL}^{-1}$ would be necessary to double the
 dose deposition for 10-100 nm diameter GNPs. In another work[4], a dose
 enhancement factor of 3.8 to 5.6 was reported for an atomic mixture of gold-
 water, and gold concentrations varying from 7 to 30 $\text{mg} \cdot \text{mL}^{-1}$, at 140 kVp
 410 (mean energy 57.9 keV). For our smallest GNP and an energy of 60 keV, we
 find enhancement ratios from 1.8 to 4.6 for 7-30 $\text{mg} \cdot \text{mL}^{-1}$, which is slightly
 lower. Besides the difference in physical models, this difference is partly due
 to the energy absorption within the GNP, which cannot be reproduced with an
 atomic mixture. Recently, Martinov *et al* [24] found, for a uniform mixture of
 415 20-100 nm diameter GNPs and water, an enhancement ratio of 3.1 and 2.7 at
 20 $\text{mg} \cdot \text{mL}^{-1}$, 20 keV. In comparison, for a 100 nm GNP, we reached a dose
 increase of 2.8.

We found that the increase of primary radiolytic yield of H_2O_2 and $\bullet\text{OH}$ is
 of the same order of magnitude as the dose increase, comprised between 6 to
 420 14 % for 1 $\text{mg} \cdot \text{mL}^{-1}$ of gold, and proportional to the gold concentration. It
 varied mostly with the photon energy mainly because of the evolution of the
 photoelectric and Compton cross sections with energy, and was maximum at

40-50 keV. Variations of the yields of a few percents were obtained with regard to the other parameters (GNP size and chemical species type). As expected, the highest yields were obtained for the smallest GNPs, as the energy lost in the GNP was minimized. At this scale, we did not observed a particularly high H_2O_2 radiolytic yield, despite the dense clusters of ionization following an Auger cascade. It must be emphasized however that the Auger contribution to the total dose is rather small. Such behavior was expected as the chemical species that are produced directly derive from the dose deposition in water.

The small enhancement of global radical production predicted at short time by our simulations suggests that the apparent overproduction obtained experimentally using coumarin scavengers [30, 33, 34, 35, 32] arise from more complex mechanisms operating over longer time. Further studies, involving in particular chemical reactions with GNPs, need to be undertaken to better understand the experimental observations. We are currently investigating such questions using MC and analytical tools, and quantum mechanical calculation [65] to better understand the kinetic of chemical reactions that may occur at the surface of GNPs, and the interaction of coumarin with GNP surface. Another perspective concerns the spatial distribution of the chemical species. While our simulations showed a minor contribution of Auger cascades to the global production of radicals, one may question whether a boost of radicals may appear close to the GNPs. This will be the presented in the second part of this work.

5. Acknowledgment

This work was supported by the LABEX PRIMES (ANR-11-LABX-0063) of Université de Lyon, within the program "Investissements d'Avenir" (ANR-11-IDEX-0007) operated by the French National Research Agency (ANR). This work has been supported by the Fondation ARC pour la recherche sur le cancer.

Appendices

450 Appendix A Track by track methodology

While the expression of the coefficients $n_i(D)$ is straightforward (see Eq. 5), the calculation of $R_{X,i}^1$ requires MC simulations. Each track t may be described by (I_0, \vec{r}_0, s) , where I_0 is the original event, defined by the photo-electron velocity and the subsequent Auger electrons velocities, \vec{r}_0 is the position of the primary photon interaction, and s is a series of random number determining totally the Markov chain. As mentioned in section 2.3.1, we decomposed the production of chemical species X , for a given irradiation dose D , as a linear combination of the chemical species produced by isolated tracks of types i , $R_{X,i}^1$, where i refers either to a track type W, W+NP and NP (i.e. 1, 2 and 3). We expose thereafter the method we used to obtain $R_{X,i}^1$, first for a photon interacting in water and then interacting in a GNP.

We define $V_W = V - X_{NP}V_{NP}$, the volume occupied by water for a total volume V containing X_{NP} (number of GNP per cm^3) of volume V_{NP} . Then, the average number of chemical species per photon interaction in water is given by,

$$R_{X,1\cup 2}^1 = \sum_{I_0, s} \int_{V_W} d\vec{r}_0 \frac{\sigma_{I_0}}{\sigma_W} \rho(\vec{r}_0) R_{X, I_0, \vec{r}_0, s}^1 \quad (\text{A1})$$

465 σ_{I_0} is the cross section for a photon interaction that leads to an initial event I_0 , σ_W is the total cross section of photon interaction in water, and, by definition, $\sum_{I_0} \frac{\sigma_{I_0}}{\sigma_W} = 1$. $\rho(\vec{r}_0)$ is the probability distribution that the initial event I_0 occurs at the position \vec{r}_0 . We assume the distribution uniform, thus $\rho(\vec{r}_0) = \frac{1}{V_W}$. $R_{X, I_0, \vec{r}_0, s}$ is the number of chemical species X induced by the track t defined by (I_0, \vec{r}_0, s) .

470

To differentiate the contributions W and W+NP, we introduce two functions,

$$\begin{cases} \delta_{I_0, \vec{r}_0, s, 1} = 1 \text{ if } t = (I_0, \vec{r}_0, s) \in T_1, 0 \text{ if } t = (I_0, \vec{r}_0, s) \in T_2 \\ \delta_{I_0, \vec{r}_0, s, 2} = 0 \text{ if } t = (I_0, \vec{r}_0, s) \in T_1, 1 \text{ if } t = (I_0, \vec{r}_0, s) \in T_2 \end{cases} \quad (\text{A2})$$

As a photon interaction in water leads either to the track type 1 or 2 (i.e. the track either interacts with a GNP or not), we find,

$$R_{X, 1 \cup 2}^1 = \sum_{I_0, s} \frac{\sigma_{I_0}}{\sigma_W} \int_{V_W} d\vec{r}_0 \left(\delta_{I_0, \vec{r}_0, s, 1} + \delta_{I_0, \vec{r}_0, s, 2} \right) \rho(\vec{r}_0) R_{X, I_0, \vec{r}_0, s}^1 \quad (\text{A3})$$

We introduce,

$$\begin{cases} P_{I_0, s, 1} = \int_{V_W} \delta_{I_0, \vec{r}_0, s, 1} \rho(\vec{r}_0) d\vec{r}_0 \\ P_{I_0, s, 2} = \int_{V_W} \delta_{I_0, \vec{r}_0, s, 2} \rho(\vec{r}_0) d\vec{r}_0 \end{cases} \quad (\text{A4})$$

475 For a track defined by an origin I_0 and the series of numbers s defining all the secondary particles, $P_{I_0, s, 1}$ (respectively $P_{I_0, s, 2}$) represents the probability that any track characterized by I_0, s has no secondary electron hitting a GNP (respectively has at least one electron hitting a GNP). Note that $P_{I_0, s, 1} + P_{I_0, s, 2} = 1$. We further introduce,

$$\begin{cases} R_{X, I_0, s, 1}^1 = \frac{1}{P_{I_0, s, 1}} \int_{V_W} d\vec{r}_0 \delta_{I_0, s, 1} \cdot \rho(\vec{r}_0) \cdot R_{X, I_0, \vec{r}_0, s}^1 \\ R_{X, I_0, s, 2}^1 = \frac{1}{P_{I_0, s, 2}} \int_{V_W} d\vec{r}_0 \delta_{I_0, s, 2} \cdot \rho(\vec{r}_0) \cdot R_{X, I_0, \vec{r}_0, s}^1 \end{cases} \quad (\text{A5})$$

480 Then Eq. A3 becomes,

$$R_{X, 1 \cup 2}^1 = \bar{R}_{X, 1}^1 + \bar{R}_{X, 2}^1 \quad (\text{A6})$$

with

$$\begin{cases} \bar{R}_{X,1}^1 = \sum_{I_0,s} \frac{\sigma_{I_0}}{\sigma_W} \cdot P_{I_0,s,1} \cdot R_{X,I_0,s,1}^1 \\ \bar{R}_{X,2}^1 = \sum_{I_0,s} \frac{\sigma_{I_0}}{\sigma_W} \cdot P_{I_0,s,2} \cdot R_{X,I_0,s,2}^1 \end{cases} \quad (\text{A7})$$

The estimation of the probability that a secondary particle hits a GNP is not straightforward when having a given number of GNPs, C_{NP} (number of particle per cm^3). We introduced the number of nanoparticles X_{NP} in the volume V ($X_{\text{NP}} = C_{\text{NP}}V$, and the probability that a track hits a GNP in a large dilution limit, $p_{I_0,s,2}$. Given a low concentration of GNP, and assuming that they are homogeneously distributed, the probability of not hitting a GNP, in the presence of X_{NP} GNPs, follows a binomial distribution,

$$P_{I_0,s,1} = 1 - P_{I_0,s,2} = \binom{0}{X_{\text{NP}}} (1 - p_{I_0,s,2})^{X_{\text{NP}}} (p_{I_0,s,2})^0 \quad (\text{A8})$$

Considering a small dose (low track density), and a low radical diffusion ($t \leq 10^{-6}$ s), the probability that a track interacts with the GNP is low, ($p_{I_0,s,2} \ll 1$). Thus, one has,

$$(1 - p_{I_0,s,2})^{X_{\text{NP}}} \sim 1 - X_{\text{NP}} p_{I_0,s,2} \quad (\text{A9})$$

Therefore, for X_{NP} GNPs in the volume V , $P_{I_0,s,1}$ and $P_{I_0,s,2}$ may be estimated with the probability that a track I_0, s hits one GNP as follows,

$$\begin{cases} P_{I_0,s,1} \sim 1 - C_{\text{NP}} \cdot V \cdot p_{I_0,s,2} \\ P_{I_0,s,2} \sim C_{\text{NP}} \cdot V \cdot p_{I_0,s,2} \end{cases} \quad (\text{A10})$$

For each track (I_0, s) generated, we estimated $p_{I_0,s,2}$, from which we derived $P_{I_0,s,1}$ and $P_{I_0,s,2}$. Concretely, to estimate $R_{X,1}^1$ (respectively $R_{X,2}^1$), we generated many primary events I_0, s is described by the seed of the pseudo-random

generator. $p_{I_0,s,1}$ and $R_{X,I_0,s,1}^1$ (respectively $R_{X,I_0,s,2}^1$) are determined for each couple I_0, s , by generating randomly numerous GNP positions in the volume V . On average and for a GNP concentration of $1 \text{ mg} \cdot \text{mL}^{-1}$, we found $P_{I_0,s,2}$ to be of the order of a few percents. Following the same approach, the probability that a generated track hit two GNPs is of the order of $P_{I_0,s,2}^2/2$. For concentrations of the order of $10 \text{ mg} \cdot \text{mL}^{-1}$, we therefore find a probability to hit one GNP of the order of 21 %, and a probability to hit two GNPs of the order of 3 %. Besides, as shown in the results section, when a track hit a GNP, the amount of energy lost in the GNP is small, and most of the energy remains deposited in water. Small probabilities combined with a small energy loss allows us to neglect the probability to hit two or more GNPs for one track and to extrapolate our results linearly with the GNP concentration up to a few tens of $\text{mg} \cdot \text{mL}^{-1}$.

For the track type NP (i.e. 3), the determination of its contribution was more straightforward. The calculation of $R_{X,3}^1$ consisted of generating a sufficient number of primary photons interaction within the GNP to reach a statistically accurate value of radiation-chemical yields.

- [1] J. F. Hainfeld, D. N. Slatkin, H. M. Smilowitz, The use of gold nanoparticles to enhance radiotherapy in mice, *Physics in Medicine & Biology* 49 (18) (2004) N309.
- [2] S. Her, D. A. Jaffray, C. Allen, Gold nanoparticles for applications in cancer radiotherapy: Mechanisms and recent advancements, *Advanced Drug Delivery Reviews* 109 (2017) 84–101.
- [3] E. Brun, C. Sicard-Roselli, Actual questions raised by nanoparticle radiosensitization, *Radiation Physics and Chemistry* 128 (2016) 134–142.
- [4] S. H. Cho, Estimation of tumour dose enhancement due to gold nanoparticles during typical radiation treatments: a preliminary monte carlo study, *Physics in Medicine & Biology* 50 (15) (2005) N163.

- [5] S. H. Cho, B. L. Jones, S. Krishnan, The dosimetric feasibility of gold nanoparticle-aided radiation therapy (gnrt) via brachytherapy using low-energy gamma-/x-ray sources, *Physics in Medicine & Biology* 54 (16) (2009) 4889.
- [6] S. X. Zhang, J. Gao, T. A. Buchholz, Z. Wang, M. R. Salehpour, R. A. Drezeck, T.-K. Yu, Quantifying tumor-selective radiation dose enhancements using gold nanoparticles: a monte carlo simulation study, *Biomedical Microdevices* 11 (4) (2009) 925.
- [7] M. Montenegro, S. N. Nahar, A. K. Pradhan, K. Huang, Y. Yu, Monte carlo simulations and atomic calculations for auger processes in biomedical nanotheranostics, *The Journal of Physical Chemistry A* 113 (45) (2009) 12364–12369.
- [8] A. Mesbahi, F. Jamali, et al., Effect of photon beam energy, gold nanoparticle size and concentration on the dose enhancement in radiation therapy, *BioImpacts: BI* 3 (1) (2013) 29.
- [9] E. Amato, A. Italiano, S. Pergolizzi, Gold nanoparticles as a sensitising agent in external beam radiotherapy and brachytherapy: a feasibility study through monte carlo simulation, *International Journal of Nanotechnology* 10 (12) (2013) 1045–1054.
- [10] N. Sinha, G. Cifter, E. Sajo, R. Kumar, S. Sridhar, P. L. Nguyen, R. A. Cormack, G. M. Makrigiorgos, W. Ngwa, Brachytherapy application with in situ dose painting administered by gold nanoparticle eluters, *International Journal of Radiation Oncology Biology Physics* 91 (2) (2015) 385–392.
- [11] B. Koger, C. Kirkby, A method for converting dose-to-medium to dose-to-tissue in monte carlo studies of gold nanoparticle-enhanced radiotherapy, *Physics in Medicine & Biology* 61 (5) (2016) 2014.
- [12] B. Koger, C. Kirkby, Optimization of photon beam energies in gold

nanoparticle enhanced arc radiation therapy using monte carlo methods,
Physics in Medicine & Biology 61 (24) (2016) 8839.

- [13] S. J. McMahon, M. H. Mendenhall, S. Jain, F. Currell, Radiotherapy in the
555 presence of contrast agents: a general figure of merit and its application to
gold nanoparticles, Physics in Medicine & Biology 53 (20) (2008) 5635.
- [14] B. L. Jones, S. Krishnan, S. H. Cho, Estimation of microscopic dose en-
hancement factor around gold nanoparticles by monte carlo calculations,
Medical Physics 37 (7Part1) (2010) 3809–3816.
- 560 [15] Z. Cai, J.-P. Pignol, N. Chattopadhyay, Y. L. Kwon, E. Lechtman, R. M.
Reilly, Investigation of the effects of cell model and subcellular location of
gold nanoparticles on nuclear dose enhancement factors using monte carlo
simulation, Medical Physics 40 (11).
- [16] M. Douglass, E. Bezak, S. Penfold, Monte carlo investigation of the in-
565 creased radiation deposition due to gold nanoparticles using kilovoltage
and megavoltage photons in a 3d randomized cell model, Medical Physics
40 (7).
- [17] A. McNamara, W. Kam, N. Scales, S. McMahon, J. Bennett, H. Byrne,
J. Schuemann, H. Paganetti, R. Banati, Z. Kuncic, Dose enhancement ef-
570 fects to the nucleus and mitochondria from gold nanoparticles in the cy-
tosol, Physics in Medicine & Biology 61 (16) (2016) 5993.
- [18] C. Kirkby, E. Ghasroddashti, Targeting mitochondria in cancer cells using
gold nanoparticle-enhanced radiotherapy: A monte carlo study, Medical
Physics 42 (2) (2015) 1119–1128.
- 575 [19] S. J. McMahon, W. Hyland, M. Muir, et al., Biological consequences of
nanoscale energy deposition near irradiated heavy atom nanoparticles, Sci-
entific Reports 1 (2011) 18.
- [20] S. J. McMahon, W. B. Hyland, M. F. Muir, J. A. Coulter, S. Jain, K. T.
Butterworth, G. Schettino, G. R. Dickson, A. R. Hounsell, J. M. O Sullivan,

- et al., Nanodosimetric effects of gold nanoparticles in megavoltage radiation therapy, *Radiotherapy and Oncology* 100 (3) (2011) 412–416.
- [21] Y. Lin, H. Paganetti, S. J. McMahon, J. Schuemann, Gold nanoparticle induced vasculature damage in radiotherapy: comparing protons, megavoltage photons, and kilovoltage photons, *Medical Physics* 42 (10) (2015) 5890–5902.
- [22] J. Schuemann, R. Berbeco, D. B. Chithrani, S. H. Cho, R. Kumar, S. J. McMahon, S. Sridhar, S. Krishnan, Roadmap to clinical use of gold nanoparticles for radiation sensitization, *International Journal of Radiation Oncology* Biology* Physics* 94 (1) (2016) 189–205.
- [23] S. Asadi, M. Vaez-zadeh, S. F. Masoudi, F. Rahmani, C. Knaup, A. S. Meigooni, Gold nanoparticle-based brachytherapy enhancement in choroidal melanoma using a full monte carlo model of the human eye, *Journal of Applied Clinical Medical Physics* 16 (5) (2015) 344–357.
- [24] M. P. Martinov, R. M. Thomson, Heterogeneous multiscale monte carlo simulations for gold nanoparticle radiosensitization, *Medical Physics* 44 (2) (2017) 644–653.
- [25] W. Ngwa, G. M. Makrigiorgos, R. I. Berbeco, Applying gold nanoparticles as tumor-vascular disrupting agents during brachytherapy: estimation of endothelial dose enhancement, *Physics in Medicine & Biology* 55 (21) (2010) 6533.
- [26] W. Ngwa, G. M. Makrigiorgos, R. I. Berbeco, Gold nanoparticle-aided brachytherapy with vascular dose painting: Estimation of dose enhancement to the tumor endothelial cell nucleus, *Medical Physics* 39 (1) (2012) 392–398.
- [27] R. I. Berbeco, W. Ngwa, G. M. Makrigiorgos, Localized dose enhancement to tumor blood vessel endothelial cells via megavoltage x-rays and targeted gold nanoparticles: new potential for external beam radiotherapy,

International Journal of Radiation Oncology Biology Physics 81 (1) (2011) 270–276.

- 610 [28] E. Amato, A. Italiano, S. Leotta, S. Pergolizzi, L. Torrisi, Monte carlo study of the dose enhancement effect of gold nanoparticles during x-ray therapies and evaluation of the anti-angiogenic effect on tumour capillary vessels, *Journal of X-ray Science and Technology* 21 (2) (2013) 237–247.
- [29] M. Laprise-Pelletier, Y. Ma, J. Lagueux, M.-F. Côté, L. Beaulieu, M.-A. Fortin, Intratumoral injection of low-energy photon-emitting gold nanoparticles: A microdosimetric monte carlo-based model, *ACS Nano* 12 (3) 615 (2018) 2482–2497.
- [30] C. Sicard-Roselli, E. Brun, M. Gilles, G. Baldacchino, C. Kelsey, H. McQuaid, C. Polin, N. Wardlow, F. Currell, A new mechanism for hydroxyl radical production in irradiated nanoparticle solutions, *Small* 10 (16) 620 (2014) 3338–3346.
- [31] M. Gilles, E. Brun, C. Sicard-Roselli, Gold nanoparticles functionalization notably decreases radiosensitization through hydroxyl radical production under ionizing radiation, *Colloids and Surfaces B: Biointerfaces* 123 (2014) 625 770–777.
- [32] M. Gilles, E. Brun, C. Sicard-Roselli, Quantification of hydroxyl radicals and solvated electrons produced by irradiated gold nanoparticles suggests a crucial role of interfacial water, *Journal of Colloid and Interface Science* 525 (2018) 31–38.
- 630 [33] N. N. Cheng, Z. Starkewolf, R. A. Davidson, A. Sharmah, C. Lee, J. Lien, T. Guo, Chemical enhancement by nanomaterials under x-ray irradiation, *Journal of the American Chemical Society* 134 (4) (2012) 1950–1953.
- [34] R. A. Davidson, T. Guo, Average physical enhancement by nanomaterials under x-ray irradiation, *The Journal of Physical Chemistry C* 118 (51) 635 (2014) 30221–30228.

- [35] R. A. Davidson, T. Guo, multiplication algorithm for combined physical and chemical enhancement of x-ray effect by nanomaterials, *The Journal of Physical Chemistry C* 119 (33) (2015) 19513–19519.
- [36] J. Chang, R. D. Taylor, R. A. Davidson, A. Sharmah, T. Guo, Electron
640 paramagnetic resonance spectroscopy investigation of radical production by gold nanoparticles in aqueous solutions under x-ray irradiation, *The Journal of Physical Chemistry A* 120 (18) (2016) 2815–2823.
- [37] E. A. Foley, J. D. Carter, F. Shan, T. Guo, Enhanced relaxation of
645 nanoparticle-bound supercoiled dna in x-ray radiation, *Chemical Communications* (25) (2005) 3192–3194.
- [38] J. D. Carter, N. N. Cheng, Y. Qu, G. D. Suarez, T. Guo, Nanoscale energy deposition by x-ray absorbing nanostructures, *The Journal of Physical Chemistry B* 111 (40) (2007) 11622–11625.
- [39] K. Butterworth, J. Wyer, M. Brennan-Fournet, C. Latimer, M. Shah,
650 F. Currell, D. Hirst, Variation of strand break yield for plasmid dna irradiated with high-z metal nanoparticles, *Radiation Research* 170 (3) (2008) 381–387.
- [40] E. Brun, L. Sanche, C. Sicard-Roselli, Parameters governing gold nanoparticle x-ray radiosensitization of dna in solution, *Colloids and Surfaces B: Biointerfaces* 72 (1) (2009) 128–134.
655
- [41] E. Brun, P. Duchambon, Y. Blouquit, G. Keller, L. Sanche, C. Sicard-Roselli, Gold nanoparticles enhance the x-ray-induced degradation of human centrin 2 protein, *Radiation Physics and Chemistry* 78 (3) (2009) 177–183.
- [42] S. J. McMahon, W. B. Hyland, E. Brun, K. T. Butterworth, J. A. Coulter,
660 T. Douki, D. G. Hirst, S. Jain, A. P. Kavanagh, Z. Krpetic, et al., Energy dependence of gold nanoparticle radiosensitization in plasmid dna, *The Journal of Physical Chemistry C* 115 (41) (2011) 20160–20167.

- [43] F. Geng, K. Song, J. Z. Xing, C. Yuan, S. Yan, Q. Yang, J. Chen, B. Kong,
 665 Thio-glucose bound gold nanoparticles enhance radio-cytotoxic targeting
 of ovarian cancer, *Nanotechnology* 22 (28) (2011) 285101.
- [44] J. Jeynes, M. Merchant, A. Spindler, A. Wera, K. Kirkby, Investigation of
 gold nanoparticle radiosensitization mechanisms using a free radical scav-
 enger and protons of different energies, *Physics in Medicine & Biology*
 670 59 (21) (2014) 6431.
- [45] P. P. Fu, Q. Xia, H.-M. Hwang, P. C. Ray, H. Yu, Mechanisms of nan-
 otoxicity: generation of reactive oxygen species, *Journal of Food and Drug*
Analysis 22 (1) (2014) 64–75.
- [46] W. Xie, W. Friedland, W. Li, C. Li, U. Oeh, R. Qiu, J. Li, C. Hoeschen,
 675 Simulation on the molecular radiosensitization effect of gold nanoparticles
 in cells irradiated by x-rays, *Physics in Medicine & Biology* 60 (16) (2015)
 6195.
- [47] H. Tran, M. Karamitros, V. Ivanchenko, S. Guatelli, S. McKinnon, K. Mu-
 rakami, T. Sasaki, S. Okada, M. Bordage, Z. Francis, et al., Geant4 monte
 680 carlo simulation of absorbed dose and radiolysis yields enhancement from a
 gold nanoparticle under mev proton irradiation, *Nuclear Instruments and*
Methods in Physics Research Section B: Beam Interactions with Materials
and Atoms 373 (2016) 126–139.
- [48] B. Rudek, A. McNamara, J. Ramos-Méndez, H. Byrne, Z. Kuncic, J. Schue-
 685 mann, Radio-enhancement by gold nanoparticles and their impact on water
 radiolysis for x-ray, proton and carbon-ion beams, *Physics in Medicine &*
Biology 64 (17) (2019) 175005.
- [49] M. Cunha, E. Testa, M. Beuve, J. Balosso, A. Chaikh, Considerations on
 the miniaturization of detectors for in vivo dosimetry in radiotherapy: A
 690 monte carlo study, *Nuclear Instruments and Methods in Physics Research*
Section B: Beam Interactions with Materials and Atoms 399 (2017) 20–27.

- [50] E. Lechtman, S. Mashouf, N. Chattopadhyay, B. Keller, P. Lai, Z. Cai, R. Reilly, J. Pignol, A monte carlo-based model of gold nanoparticle radiosensitization accounting for increased radiobiological effectiveness, *Physics in Medicine & Biology* 58 (10) (2013) 3075.
- [51] E. Lechtman, J.-P. Pignol, Interplay between the gold nanoparticle sub-cellular localization, size, and the photon energy for radiosensitization, *Scientific Reports* 7 (1) (2017) 13268.
- [52] P. Retif, A. Reinhard, H. Paquot, V. Jouan-Hureau, A. Chateau, L. Sancey, M. Barberi-Heyob, S. Pinel, T. Bastogne, Monte carlo simulations guided by imaging to predict the in vitro ranking of radiosensitizing nanoparticles, *International Journal of Nanomedicine* 11 (2016) 6169.
- [53] Y. Frongillo, T. Goulet, M. Fraser, V. Cobut, J. Patau, J. Jay-Gerin, Monte carlo simulation of fast electron and proton tracks in liquid water-ii. non-homogeneous chemistry, *Radiation Physics and Chemistry* 51 (3) (1998) 245–254.
- [54] B. Gervais, M. Beuve, G. Olivera, M. Galassi, Numerical simulation of multiple ionization and high LET effects in liquid water radiolysis, *Radiation Physics and Chemistry* 75 (2006) 495–513.
- [55] F. Poignant, B. Gervais, A. Ipatova, C. Oleg, L. Pierre-Jean, E. Testa, M. Beuve, Theoretical derivation and benchmarking of cross sections for low-energy electron transport in gold, *European Physical Journal Plus* Under revision.
- [56] V. Tessaro, F. Poignant, M. Beuve, B. Gervais, M. Galassi, Theoretical study of w-values for particle impact on water, *Nuclear Instruments and Methods in Physics*.
- [57] W. Li, A. Belchior, M. Beuve, Y. Chen, S. D. Maria, W. Friedland, B. Gervais, B. Heide, N. Hocine, A. Ipatov, A. Klapproth, C. Li, J. Li, G. Multhoff, F. Poignant, R. Qiu, H. Rabus, B. Rudek, J. Schuemann,

- 720 S. Stangl, E. Testa, C. Villagrasa, W. Xie, Y. Zhang, Intercomparison of
dose enhancement ratio and secondary electron spectra for gold nanoparti-
cles irradiated by x-rays calculated using multiple monte carlo simulation
codes, *Physica Medica* 69 (2020) 147–163.
- [58] A. Colliaux, B. Gervais, C. Rodriguez-Lafrasse, M. Beuve, Simulation of
725 ion-induced water radiolysis in different conditions of oxygenation, *Nuclear
Instruments and Methods in Physics Research Section B: Beam Interactions
with Materials and Atoms* 365 (2015) 596–605.
- [59] M. Berger, J. Hubbell, S. Seltzer, J. Chang, J. Coursey, R. Sukumar,
D. Zucker, K. Olsen, XCOM: Photon cross section database (version 1.5),
730 National Institute of Standards and Technology.
- [60] W. R. Leo, *Techniques for nuclear and particle physics experiments: a
how-to approach*, Springer Science & Business Media, 2012.
- [61] H. Ouerdane, B. Gervais, H. Zhou, M. Beuve, J.-P. Renault, Radiolysis of
water confined in porous silica: a simulation study of the physicochemical
735 yields, *The Journal of Physical Chemistry C* 114 (29) (2010) 12667–12674.
- [62] A. Colliaux, B. Gervais, C. Rodriguez-Lafrasse, M. Beuve, O₂ and glu-
tathione effects on water radiolysis: a simulation study, in: *Journal of
Physics: Conference Series*, Vol. 261, IOP Publishing, 2011, p. 012007.
- [63] H. Yamaguchi, A spur diffusion model applied to estimate yields of species
740 in water irradiated by monoenergetic photons of 50 ev–2 mev, *International
Journal of Radiation Applications and Instrumentation. Part C. Radiation
Physics and Chemistry* 34 (5) (1989) 801–807.
- [64] E. Lechtman, N. Chattopadhyay, Z. Cai, S. Mashouf, R. Reilly, J. Pignol,
745 Implications on clinical scenario of gold nanoparticle radiosensitization in
regards to photon energy, nanoparticle size, concentration and location,
Physics in Medicine & Biology 56 (15) (2011) 4631.

- [65] C.-H. Chan, F. Poignant, M. Beuve, E. Dumont, D. Loffreda, A water solvation shell can transform gold metastable nanoparticles in the fluxional regime, *The Journal of Physical Chemistry Letters* 10 (5) (2019) 1092–1098.

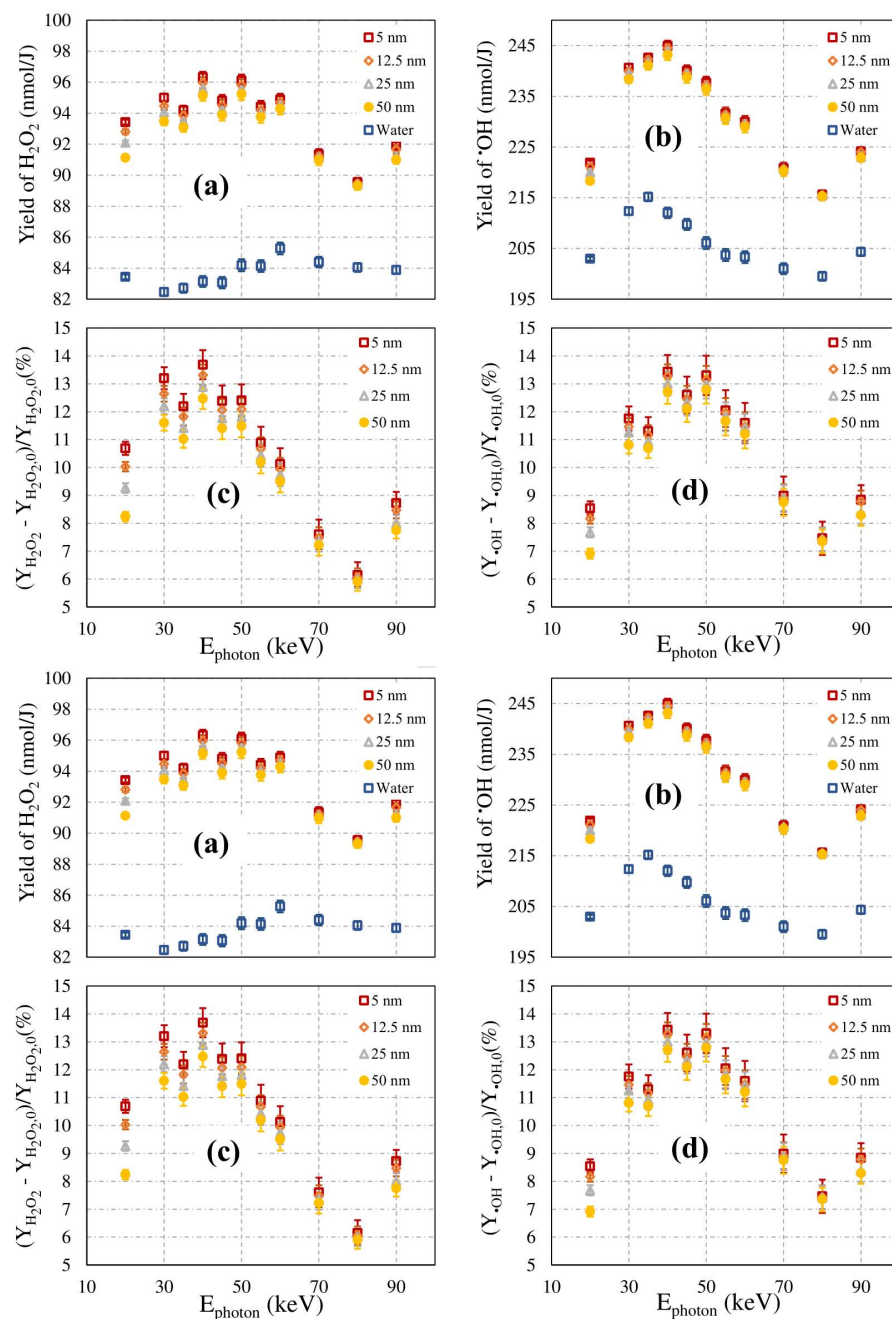


Figure 4: H_2O_2 and $\bullet\text{OH}$ yield dependence upon primary photon energy for different R_{NP} and pure water at 10^{-6} s. The GNP concentration C_{GNP} was set at $1 \text{ mg} \cdot \text{mL}^{-1}$. On top, yields are in $\text{nmol} \cdot \text{J}^{-1}$ while on the bottom, relative enhancements with regard to the yield in the absence of GNPs are in %.

- We calculate radiolytic yields of free radicals for low-energy (20-90 keV) photon irradiation of gold nanoparticle water solution.
- 1mg/mL of GNPs increases radical production from 6 to 14 %.
- Radical production enhancement is similar to the dose enhancement.

Declaration of interests

☒ The authors declare that they have no known competing financial interests or personal relationships that could have appeared to influence the work reported in this paper.

☐ The authors declare the following financial interests/personal relationships which may be considered as potential competing interests:

--